Article

The changing nature of future Arctic marine heatwaves and its potential impacts on the ecosystem

Ruijian Gou [1,2] ✉, Klara K. E. Wolf [3,4], Clara J. M. Hoppe [2], Lixin Wu [1,5] & Gerrit Lohmann [2,6]

Marine heatwaves (MHWs), defined as extreme ocean warming episodes, have strengthened over the past decades. High-resolution climate models improve understanding of MHWs under global warming, but such events in the future Arctic are currently overlooked. In a high-resolution climate model, we find Arctic MHWs intensify on orders of magnitude during the warming twenty-first century, following sea ice retreat. However, with little sea ice coverage, strong interannual variability emerges, which could surpass the amplitude of former intensification. Furthermore, the enhancement of MHWs correlates with an order of magnitude increase in the rate of change in the temperature anomaly. Additionally, MHWs are found to be accompanied by stratification enhancement, which could surpass interannual variability of future stratification. Such extreme temperature fluctuations combined with stratification enhancement suggest major challenges for Arctic ecosystems, and may negatively impact food webs through direct physiological temperature effects, as well as indirectly through nutrient supply and taxonomic shifts.

Marine heatwaves (MHWs) have received public attention as a result of their severe harm to ecosystems[1]. MHWs are predicted to be more intense and persistent under future global warming, and thus the impact on marine ecosystems will be inevitably enhanced[2–4].

However, a missing aspect of MHW studies is their future development in the Arctic. The Arctic Ocean is the only ocean basin with large areas of sea ice cover. It is warming much faster than any other ocean, a phenomenon known as Arctic amplification[5], and is rapidly losing its sea ice cover[6]. Underneath the sea ice, temperatures are relatively constant (although increases of 0.4 °C by penetrating shortwave radiation have been described[7]), because sea ice largely prevents the atmospheric warming from entering the ocean. But as sea ice retreats and air–sea interactions increase, MHWs can increasingly emerge, and the concomitant environmental changes may be unprecedented for the modern climate.

Observational records indicate an increase in the intensity of Arctic MHWs[8,9] in various Arctic basins[10–13]. The intensification mainly follows sea ice decline in summer[8,13] and is attributed to both stronger stratification and solar heat input[8]. While others[8] predicted that Arctic MHWs will continue to intensify as summer sea ice decreases, little is known about future variability.

Observations of ecological impacts of MHWs in the high-latitude regions are still rare and rely on opportunistic descriptions mainly of conspicuous long-term events[14–17]. Here, we provide a collection of the present literature on the potential ecological impacts of those MHW properties that can be meaningfully assessed in the scope of this physical model, to guide future modelling studies to be more applicable to field and experimental studies on MHW effects. In the few existing observations in polar regions (mainly the Southern Ocean), MHWs

[1]Frontiers Science Center for Deep Ocean Multispheres and Earth System and Key Laboratory of Physical Oceanography, Ocean University of China, Qingdao, China. [2]Alfred Wegener Institute, Helmholtz Centre for Polar and Marine Research, Bremerhaven, Germany. [3]Institute of Marine Ecosystem and Fishery Science, Universität Hamburg, Hamburg, Germany. [4]Limnological Institute, University of Konstanz, Konstanz, Germany. [5]Laoshan Laboratory, Qingdao, China. [6]University of Bremen, Bremen, Germany. ✉e-mail: rgou@foxmail.com

often lead to increased chlorophyll *a* concentrations, interpreted as increased production[18] (but see ref. [19]), which is in contrast to the observed chlorophyll *a* decrease during lower-latitude MHWs[4]. This may be explained by the dependence of MHW effects on the nutrient regime, with MHW stimulating primary production in high-nutrient regimes and productivity decreases in nutrient-limited regions[4,20,21]. Long-term, warm-water anomalies have been described to have large-scale and cascading food web effects, including northwards shifts of species, changed migration patterns and even mass die-offs caused by toxic algal blooms or starvation[4,17,22]. Such dramatic events are often connected to changes in stratification or upwelling dynamics that impoverish the nutrient regime of primary producers, which then propagate through the entire food web[16,21].

High-resolution climate models better capture the extreme events and open a new field for the study of MHWs under climate change. The turbulent motions and small-scale air–sea interactions in high-resolution models increase the intrinsic variability of the climate system, leading to more extreme conditions[23,24]. Congruently, high-resolution models have been shown to simulate stronger and more realistic MHWs than coarse-resolution models[25,26]. As the resolution increases, the gap of underestimated MHWs in models compared to observations decreases[25,26]. Thus, the future variability of MHWs can best be studied by the climate model with the highest resolution available. In this study, we use a cutting-edge high-resolution climate model to evaluate the variability of Arctic MHWs and their potential ecological impacts in the warming twenty-first century. The nominal resolution of this model is 0.1° in the ocean and 0.25° in the atmosphere[27], which is high compared to other publicly available climate models[28].

In the context of future variability, the definition of the threshold for MHWs is a key aspect. The threshold is usually defined by the seasonally varying 90th percentile of local sea surface temperature (SST) during a baseline period[29]. Owing to the limited time span (about four decades) of observational data, the baseline periods of observational studies are generally the entire time span. In climate models for future warming scenarios, some studies use a similar historical baseline period[2,3]. In a warming climate, however, using such a fixed type of baseline for MHWs can inflate their occurrence and intensity, since it captures both the generally warming climate and the extreme variability[1]. A strengthening trend of MHWs could thus be mainly caused by the increase in mean SST[30,31]. Furthermore, for many ecosystem components, considerable adaptation to the long-term SST increase is to be expected (either through evolution or range shifts[32]) and it is unlikely that a future ecosystem will have the same sensitivity to short-term temperature increases as a current or past one. We therefore focus on MHWs induced only by extreme variability and remove the impact of rising mean SST by applying a 31-year moving-baseline period around the target year.

The changing nature of Arctic MHWs

Owing to the strong seasonality in the Arctic, primary production is largely limited to summer (June, July and August (JJA))[33,34], making it the most productive period of the Arctic ecosystem[21]. In the central Arctic in September, irradiances decrease quickly and nutrients are usually depleted, preventing major biomass development even in ice-free locations. Summer (JJA) is also the season when the intensity of MHW is most pronounced in both observational[8] and future periods (Extended Data Fig. 1). Therefore, we focus on MHWs during the summer season (JJA) and in the surface ocean (5 m), as this layer is where primary production is mostly occurring.

The range of cumulative intensity of Arctic MHWs in the model is close to observational MHWs (Fig. 1), in terms of both spatial and temporal patterns, showing that the model can reproduce the observed amplitude of extreme variabilities. The same conclusion also applies to comparisons in cumulative duration and frequency (Extended Data Figs. 2 and 3). A difference between model and observations is the

maximum intensity, which is ~0.5 °C weaker in the model (Extended Data Fig. 4). We mask the observational area of sea ice cover and only compare the time series of low sea ice presence, since the observational dataset calculates under-ice temperature on the basis of a parameterization that results in barely any variability, while the model allows such variability. The time series during the observational time period in the model cannot correspond in phase with the observational time series, as the MHWs are featured with intense interannual variability to be discussed below. For more information about the model skills, please refer to the Methods.

The applied warming scenario (representative concentration pathways (RCP) 8.5; Methods) is characterized by atmospheric CO_2 concentration increasing from ~300 to 800 ppm in 1965–2085, inducing rapid global warming (Fig. 2a). The corresponding Arctic SST increase in summer is nearly 7 °C, more than twice the average global warming of 3 °C (Fig. 2b). Across the entire modelled timeframe, there are two types of trends of MHWs under global warming (Fig. 2)—an increase of MHWs following sea ice retreat and a pronounced interannual variability in areas of low sea ice cover. We will discuss these patterns separately below.

The greatest cumulative intensity of MHWs is observed where sea ice has substantially retreated close to the continents (Fig. 2c). This positive long-term trend of intensifying MHWs after sea ice retreat (Fig. 2d) is consistent with the historical changes that also show strengthening of MHWs near the sea ice edge[8]. The hardly intensifying trend where sea ice concentration (SIC) decreases is related to the intense interannual variability to be discussed in the following. As the sea ice extent continues to shrink towards the North Pole in the future, the newly exposed sea surface will be subject to stronger MHWs, potentially further destabilizing the formerly ice-covered Central Arctic ecosystem.

When the sea ice cover of a given region decreases sharply (for example, to SIC < 50%) or is barely present, MHWs in that region not only become more intense, but also vary strongly on an interannual timescale (Fig. 2e). The strong interannual variability of MHWs at lower sea ice cover is related to the onset of air–sea interaction (in the absence of sea ice), which has also contributed to the observed interannual variability of MHW in the Barents Sea[10] and Bering Seas[11]. The amplitude of the interannual variability in the model is close to the observational results (Fig. 1c).

We argue that the observed enhancement of Arctic MHWs seen in recent decades[9] along the sea ice edge is partly due to sea ice retreat itself, but that in regions where sea ice cover is constantly <15%, observations of increased MHW intensity reflect interannual variability rather than a signal of sea ice retreat. The model suggests that there are years when MHWs substantially intensify and then weaken as a result of interannual variability. The mechanisms modulating this interannual variability need further investigation and are beyond the scope of our study.

Overall, in the near-term future, when the Arctic is still mostly covered by sea ice, the sea ice retreat will be the dominant cause for the intensification of MHWs. However, once the Arctic has lost its (summer) sea ice cover, MHW dynamics in the Arctic will be controlled by interannual variability caused by air–sea interactions.

Other properties of MHWs relevant for ecosystem functioning include cumulative duration, frequency, duration per MHW and maximum intensity. Please refer to the Methods for their detailed definitions and description. These properties should be considered when designing experiments studying the ecological and physiological impacts of Arctic MHWs. Next, we discuss the key properties that could have direct effects on biology.

Abruptness and potential direct ecological impacts

Amplified MHWs challenge organisms' abilities to acclimate not only to periods of extremely high temperatures, but also to very fast temperature fluctuations. The rate of temperature anomaly change (above
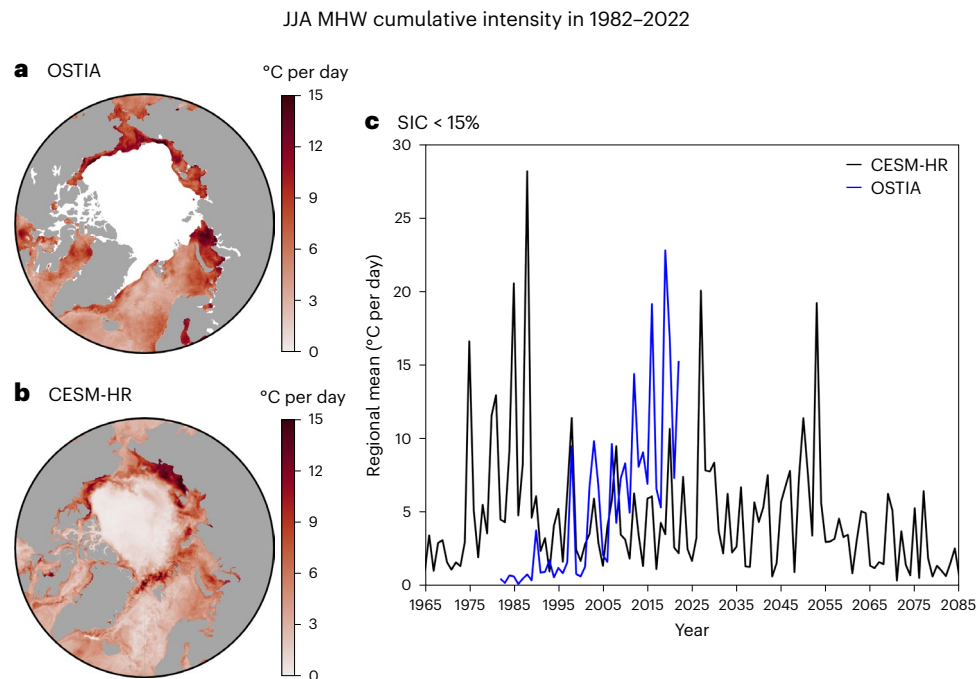
JJA MHW cumulative intensity in 1982–2022

Fig. 1 | The cumulative intensity of Arctic MHWs in the observational record. **a,b**, The average over the summer seasons (JJA) in 1982–2022 for observational dataset (**a**) and the model (**b**). The observational area with SIC > 15% at the end of summer season (average on 31 August) is masked by white shading. **c**, Time series of the JJA-mean cumulative intensity, averaged over regions with SIC < 15%. The standard deviations of the time series from the model and observational dataset are, respectively, 4.40 and 5.72 °C per day.
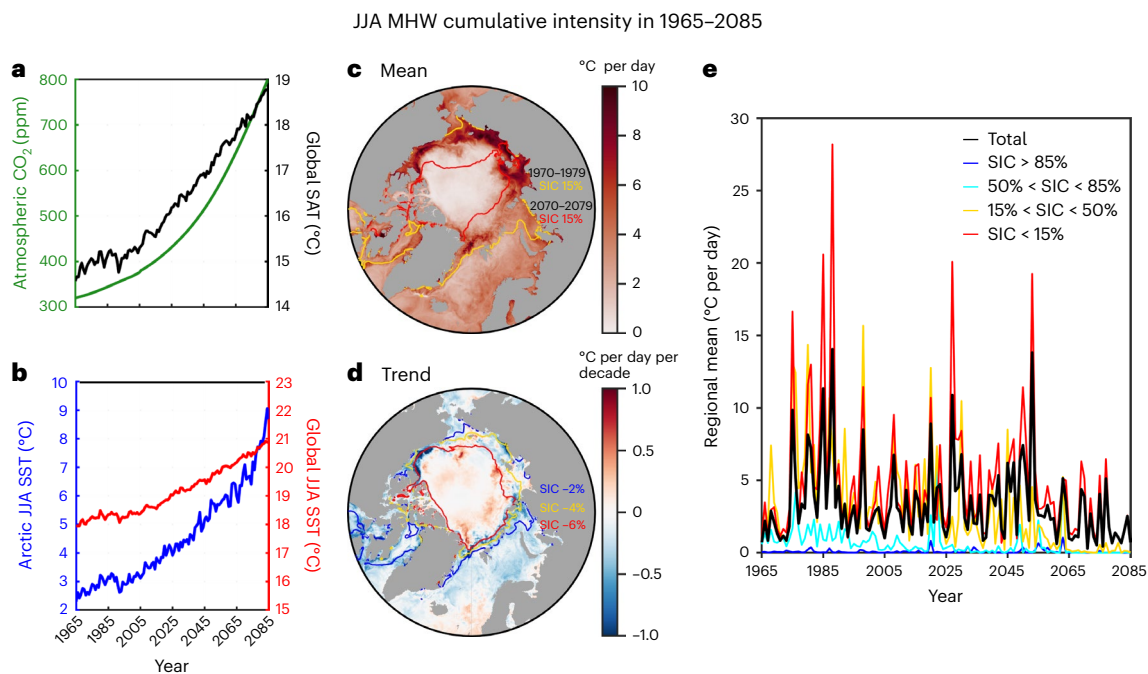
JJA MHW cumulative intensity in 1965–2085

Fig. 2 | The cumulative intensity of Arctic MHWs under global warming in a high-resolution climate model. a, The global average of atmospheric CO_2 concentration (green line) and surface air temperature (black line). **b**, Summer SST averaged over the Arctic (north of 60° N, blue line) and global ocean (red line). **c–e**, Mean state (**c**), linear decadal trend (**d**) and time series (**e**) of the cumulative intensity of MHWs over JJA in 1965–2085. The time series are (annual means) averaged over regions with certain SIC, denoted by lines of different colour in **e**. The yellow and red lines in **c** indicate the SIC of 15% averaged over 1970–1979 and 2070–2079, respectively. The blue, yellow and red lines in **d** indicate the linearly decreasing decadal trends of 2%, 4% and 6%, respectively.

the climatological threshold of MHWs) during the development and decay phases of MHWs can be described as the abruptness of warming and cooling. We find that the abruptness of SST anomaly change is similar during development and decay phases. Therefore, we only discuss the development phase of MHWs, while the results also apply to the decay phase.

As an exemplary case study, we select the two MHW events with the largest maximum intensity at a model grid cell (green dot in Fig. 3d)
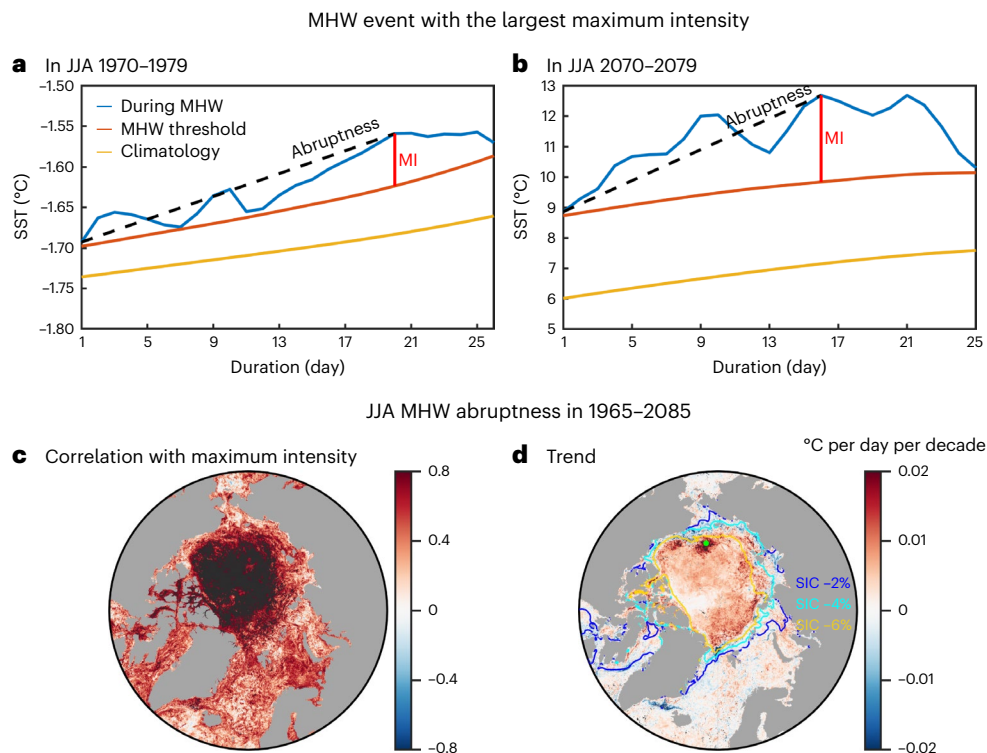
MHW event with the largest maximum intensity

JJA MHW abruptness in 1965–2085

Fig. 3 | The abruptness of temperature change during the development phase of MHWs in a high-resolution climate model. a, The SST during an MHW event as well as the MHW threshold and SST climatology at the green dot shown in **d**. The MHW event has the greatest maximum intensity in the summer of 1970–1979. The SST climatology is defined as the average over the days used to define the threshold. **b**, The same as **a** but for the summer of 2070–2079. **c**, Correlation between the abruptness and maximum intensity of MHWs in JJA from 1965 to 2085. **d**, Linear decadal trend of the abruptness over JJA in 1965–2085. The yellow, cyan and blue lines in **d** show linearly decreasing decadal trend of 2%, 4% and 6%, respectively, for the SIC. MI, maximum intensity.

during the summers of 1970–1979 and 2070–2079, respectively. Note that sea ice largely covers this location in the central Chukchi Sea in the first period, but has disappeared (<15%) in the second period (Fig. 2c,d). With this reduction in sea ice cover, the maximum intensity as well as the abruptness of the MHW are an order of magnitude greater in the future event than in the past one. More specifically, the maximum intensity increases from <0.1 to >3 °C, with SST exceeding the climatology by almost 6 °C, while the abruptness correspondingly changes from <0.1 °C in 20 days to >3 °C in 16 days (on average 0.005 and 0.2 °C per day, respectively). The case study thus illustrates impressive increases in both intensity and abruptness.

Abruptness is also strongly correlated with maximum MHW intensity for the Arctic as a whole (Fig. 3c). Since the duration per MHW shows much less variability compared to their maximum intensity (Extended Data Figs. 5c and 6c), considering the definition of abruptness, the future change of abruptness is largely determined by the maximum intensity. Concurrently, the spatial pattern (Fig. 3d) of the trend in abruptness is similar to that of maximum intensity (Extended Data Fig. 6b)—the largest increase is detected in the central Arctic, where sea ice cover is substantially reduced. The average abruptness increase in the next century is 0.057 °C per day at locations where SIC decreases by >60% (Fig. 3d), with a corresponding increase in maximum intensity around 1 °C. With sea ice retreat, the increase of abruptness would be orders of magnitude higher, corresponding to the increases of maximum intensity (Extended Data Fig. 6c).

The combination of intense and abrupt heatwave events is likely to pose large challenges on Arctic cold adapted organisms, as conditions may approach or even surpass their physiological boundaries while limiting the time they have for physiological acclimation. Importantly, such direct temperature effects can impact all trophic levels simultaneously (Fig. 6a). Warming is known to increase metabolic rates in

general[35,36], which may translate into higher primary productivity in the short term if nutrients are available[37], but also indicate higher food requirements and activity by grazers and predators[38–40]. Depending on the severity of the MHW, the organism's environmental history[41,42] and adaptive flexibility, such physiological challenges may have more or less pronounced detrimental consequences, but will certainly make organisms more susceptible to additional stressors. Since respiration is more temperature-sensitive than photosynthesis[43], increases in heterotrophic process and net community respiration are likely[19,44]. Sudden temperature increases may also cause imbalances in cell homeostasis and metabolism[45], impact recruitment success[46] and increase the accumulation of reactive oxygen species[47]. Arctic marine organisms (especially those from higher trophic levels) are particularly sensitive to high temperatures and oxidative stress, since they are adapted to low metabolic rates and thus low levels of reactive oxygen species[48]. For one of the most abundant zooplankton species in the Arctic Ocean, *Calanus glacialis*, 6 °C has been shown to be the upper limit of the fundamental thermal niche[45,49], potentially setting a boundary to MHW survival. If MHW effects impact different trophic levels to a different degree or on different time frames, trophic mismatches between predator and prey populations can develop[50,51], especially when organismal groups with complex life cycles are involved. Changes in species composition are thus likely on all trophic levels, but especially quickly on the lower levels given their shorter generation times. They could include shifts towards more heat-tolerant taxa, including invading and toxic species (borealization and harmful algal blooms[52,53]), but also biodiversity loss, which may reduce overall resilience to further disturbances or even to the return to cool temperatures at the end of the MHWs. The effects of the cooling after an MHW are indeed hardly investigated[37]. Especially if selective shifts have taken place, it is likely that the system will not simply return to its former state, or take a long time to do so[54]. Even
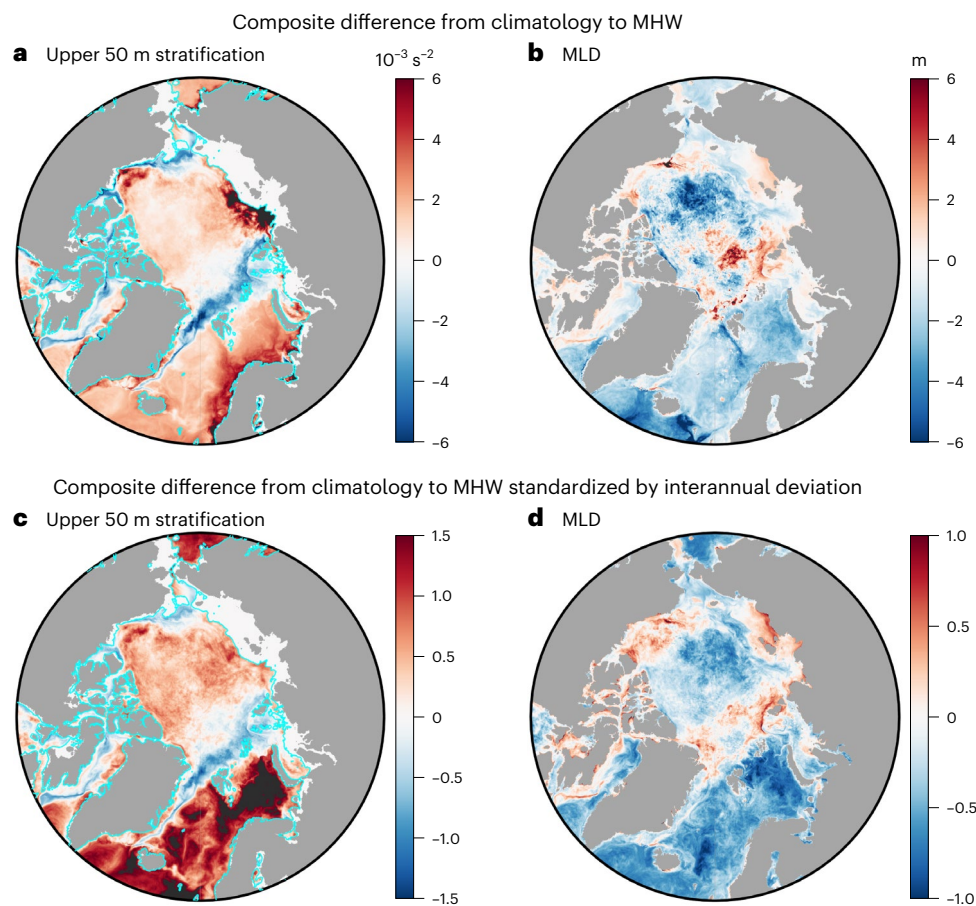
Fig. 4 | The change of stratification and MLD with MHWs. a,b, The composite-mean change (per day) of stratification in the upper 50 m (a) and MLD (b) from daily climatology to MHW days. All the MHW days during JJA 1965–2085 are composited. The daily climatology is defined as the average over the days of the same MHW dates in the 31 year moving-baseline period. c,d, As in a (c) and b (d) but standardized by interannual standard deviation. The interannual standard deviation is based on the same days as the daily climatology. The MLD is a direct model output. The cyan contours denote 50 m isobaths and, at where the depth is shallower than 50 m, no daily stratification values are available.

physiologically, carry-over effects of heat stress can still influence the state of organisms after an MHW has passed[55,56], and the cooling after acclimation to warmer conditions may act as an additional stressor, causing further metabolic imbalances and detrimental responses[57].

Stratification and potential indirect ecological impacts

Arctic MHWs can also have indirect effects on ecosystems, primarily through increased ocean stratification. This can be illustrated with the composite-mean change in the upper 50 m stratification and mixed layer depth (MLD) from climate background state to MHW (Fig. 4). Compared to the climatology, stratification generally increases and MLD decreases during a MHW. In the Southern parts of the European Arctic, where there is no summer sea ice, the stratification during MHWs could increase to being above the interannual variability (Fig. 4c,d). In some limited regions, however, a decrease in stratification and increase in MLD could be observed in the model (Methods).

While the increase in temperature during MHWs can directly induce elevated stratification[58], increased meltwater and freshwater runoff during warm periods strongly controls stratification in polar surface oceans, which in turn can stimulate and enhance MHWs in surface waters[8,59]. As seen in mean-state changes in the effects of temperature and salinity on stratification (Fig. 5), the influence of temperature on stratification increases while the salinity effect decreases where sea ice has retreated (Figs. 2c and 5a,b,e,f). Given that the stratification control index (SCI) increases to above −1, the Arctic Ocean can thus be expected to shift to a state that is stratified by both temperature and salinity (Fig. 5i,j). Although stratification in the Arctic Ocean is currently generally determined by salinity[60], as is also the case in the early period of model (Fig. 5), we expect that temperature will increasingly affect stratification.

The declining effect of salinity suggests that meltwater and runoff have less important roles in inducing future MHWs in this region (Fig. 5e,f). Furthermore, our results indicate that the SCI anomaly during MHWs could reach values of 1, with highest values towards the central Arctic. To summarize, our results suggest that stratification can be substantially enhanced on short time scales by strong MHWs, although further investigations are necessary to better quantify and generalize this effect.

The potential indirect MHW effects on the ecosystem, such as increased stratification, are mainly driven by the bottom of the food web through changes in primary production, and account for a large proportion of the MHW impacts currently described in the literature[61]. A shallower mixed layer causes cells to spend more time under higher irradiances, but also impedes nutrient supply from deeper water layers[58,62] (Fig. 6b). Over time this is likely to lead to nutrient limitation and a concurrent decline in primary production, as can also be expected from increased freshwater inputs to the Arctic, potentially exacerbating each others detrimental effects. The concurrent shift towards smaller species with higher nutrient-uptake efficiency[58] can have major consequences for higher trophic levels, as such smaller species often have lower carbon export rates to depth[63]. Even though large parts of the central Arctic Ocean are already now rather oligotrophic and dominated by picoplankton[64,65], these patterns can be
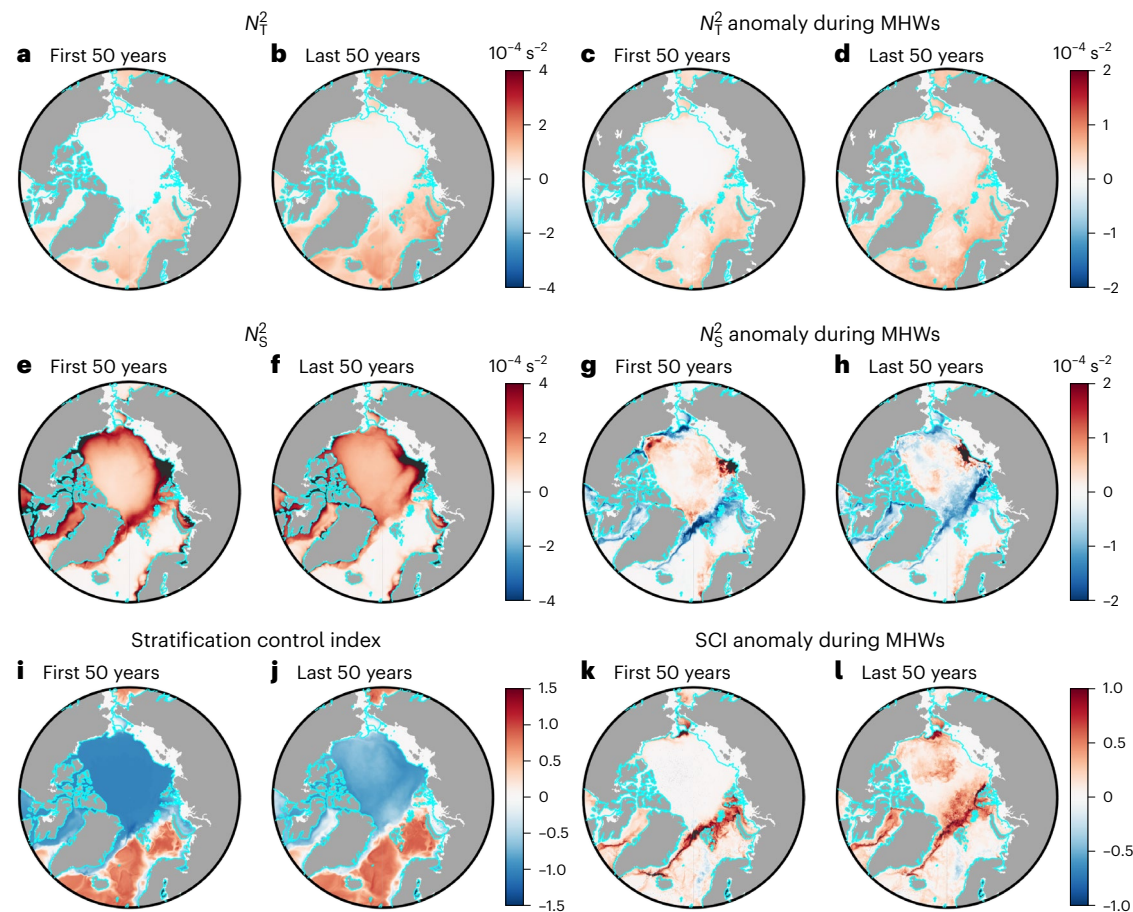
Fig. 5 | The change of temperature and salinity effects on the upper 50 m stratification. a,b, The mean state of temperature effect on stratification in the first (**a**) and last (**b**) 50 years in JJA 1965–2085. **c,d**, The composite-mean change (per day) of temperature effect on stratification from daily climatology to MHW days in the first (**c**) and last (**d**) 50 years in JJA 1965–2085. **e–h**, As in **a–d** but for the salinity effect on stratification. **i–l**, As in **a–d** but for the SCI that measures relative contributions from temperature and salinity on stratification (section on 'Stratification' in Methods). The cyan contours denote 50 m isobaths.

expected to intensify during MHWs, impeding pulses of nanoplankton production during mixing or upwelling events. Mechanistically similar responses have been described during several ocean warming events, where reduced upwelling or mixing caused a shift of species towards smaller phytoplankton[66,67]. Effects of such changes can cascade up the food web, by favouring smaller, less nutritious, zooplankton, which in turn can cause mass starvation events at the level of higher predators, such as seabirds, fish and mammals[68,69]. Once such deep-rooting ecosystem changes have taken place, the recovery after a MHW is often slow or the system shifts to new equilibria[14,70]. Underlying processes are, however, heavily dependent on the specifics of location and the extreme event[20], which makes general mechanisms hard to identify and requires more dedicated experiments and observations. Given that the summertime Arctic Ocean is largely nutrient limited now[71,72], the additional MHW-driven reduction in nutrient replenishment may be small in absolute terms, but may strongly affect an ecosystem already existing in a strongly limited setting in relative terms.

Not only nutrients but also other biogeochemical components of the high Arctic system may be affected by MHWs. As for carbonate chemistry, the Arctic exhibits particularly fast ocean acidification[73], with parts of the Arctic already being undersaturated in aragonite[74]. While Arctic phytoplankton has been shown to be rather resilient to combined warming and ocean aciditification[75], their sensitivity may be modulated under nutrient-limited conditions that can be expected to co-occur. Effects of MHWs on ocean acidification are not easy to project, as warmer temperatures cause higher [H+] due to changes in the equilibrium of the carbonate chemistry, but can also cause outgassing of CO_2 due to lower solubility, potentially reversing the former effect[76]. As aragonite and calcite undersaturation are less likely under warmer conditions[74], and as the few available data suggest a dominance of the latter mechanism[76], MHWs do not seem to further aggravate ocean acidification in the Arctic Ocean.

As another indirect effect, enhanced sea ice melt under MHW conditions may also cause habitat loss of sea ice algae, which can contribute substantially to primary productivity in the central Arctic Ocean[77,78], thereby reducing the productive season of this habitat with potentially negative implications for higher trophic levels[79]. Overall, a large number of different preconditions as well as direct and indirect MHW effects in concert will determine the overall ecosystem response.

Summary and conclusions

In summary, the characteristics and trends of future Arctic MHWs based on our cutting-edge high-resolution climate model can guide assessments of the expected ecosystem impacts, for example via more targeted design of experiments and observation campaigns. We highlight that Arctic MHWs intensify by orders of magnitude in the twenty-first century following sea ice retreat, and that the intensity of MHWs in areas with low sea ice cover exhibits strong interannual variability. The intensification of MHWs is accompanied by increasing abruptness of temperature changes and stratification developing in the Central Arctic. The increase of extreme temperature fluctuations and stratification has the potential to alter the Arctic ecosystem, with probable increasingly unfavourable conditions for Arctic productivity and the current configuration of the ecosystem.
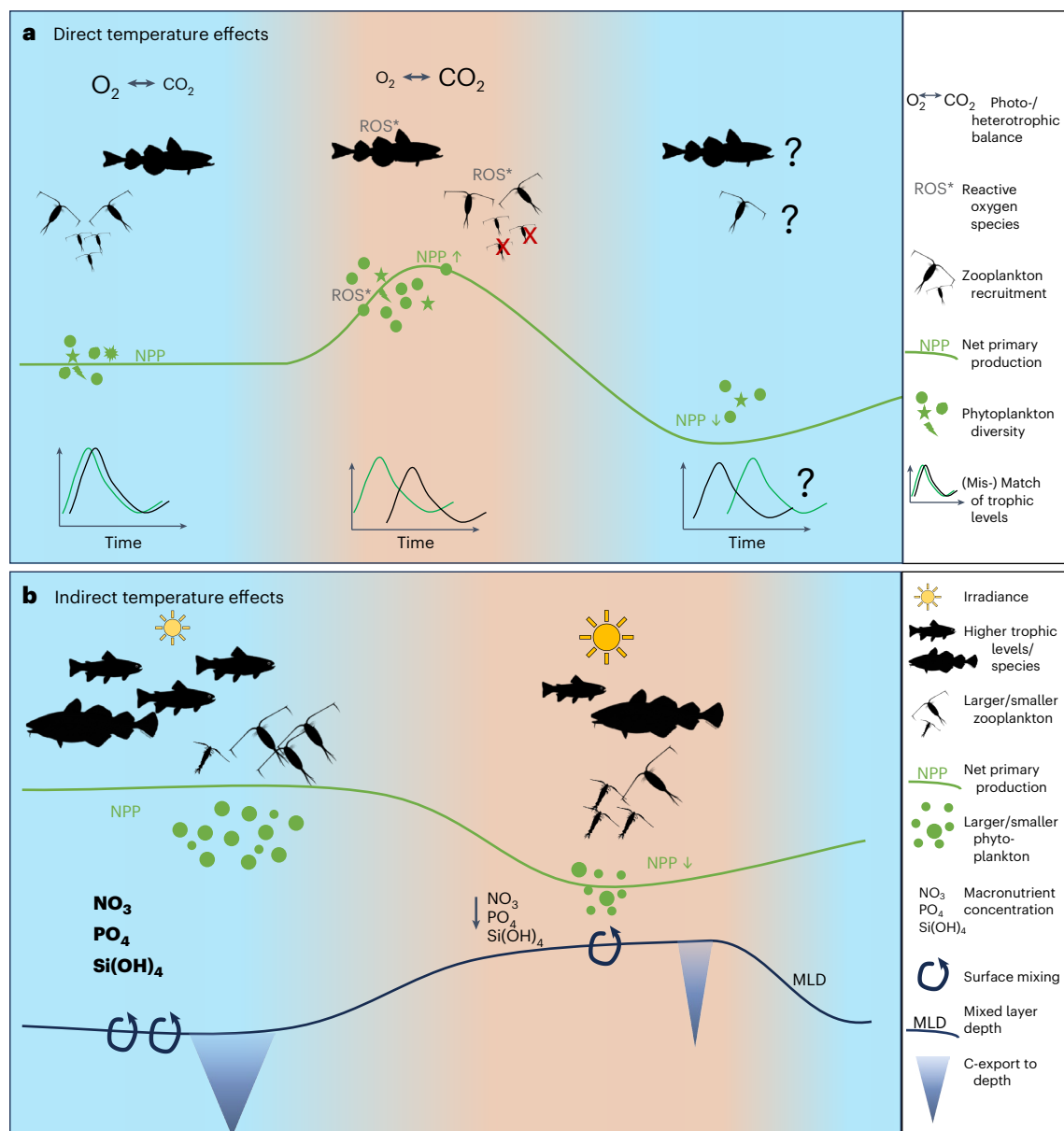
Fig. 6 | Conceptual diagrams illustrating the potential effects on biology induced by Arctic MHWs. a, Potential direct temperature effects under non-limiting nutrient conditions include an increase of net primary production (NPP), but a stronger increase in respiration of all organisms. This may cause the system to shift towards net heterotrophy (that is, to producing more CO_2 than O_2). A concurrent increase in oxidative stress (ROS) in heat-stressed organisms may indicate increased mortality and decreased recruitment success. Shifts in species composition and life-stage timing may also cause temporal mismatches between producers and consumers. Extremely little is still known about responses to the cool phase after a heatwave, especially for higher trophic levels. **b**, Potential indirect temperature effects are driven by increased thermal stratification and reduced MLD, increasing mean surface irradiance, but reducing nutrient (NO_3, PO_4 and $Si(OH)_4$) input to the upper ocean layers. This may cause reduced NPP, species shifts on all trophic levels and less carbon (C) export to depth.

To explore the specific impacts of MHWs on ecosystems under climate change would require high-resolution climate models coupled with similarly sophisticated models for biology, which are currently not available. Developing such high-resolution coupled models is indeed urgently needed and could greatly improve our understanding and prediction of Arctic ecosystems under climate change by incorporating their responses to increasingly impactful extreme events.

Online content

Any methods, additional references, Nature Portfolio reporting summaries, source data, extended data, supplementary information, acknowledgements, peer review information; details of author contributions

and competing interests; and statements of data and code availability are available at https://doi.org/10.1038/s41558-024-02224-7.

References

1. Oliver, E. C. et al. Marine heatwaves. *Annu. Rev. Mar. Sci.* **13**, 313–342 (2021).
2. Frölicher, T. L., Fischer, E. M. & Gruber, N. Marine heatwaves under global warming. *Nature* **560**, 360–364 (2018).
3. Oliver, E. C. et al. Longer and more frequent marine heatwaves over the past century. *Nat. Commun.* **9**, 1324 (2018).
4. Cavole, L. M. et al. Biological impacts of the 2013–2015 warm-water anomaly in the Northeast Pacific—winners, losers, and the future. *Oceanography* **29**, 273–285 (2016).

5. Serreze, M. C., Barrett, A. P., Stroeve, J. C., Kindig, D. N. & Holland, M. M. The emergence of surface-based Arctic amplification. *Cryosphere* **3**, 11–19 (2009).

6. Meier, W. N. & Stroeve, J. An updated assessment of the changing Arctic sea ice cover. *Oceanography* **35**, 10–19 (2022).

7. Maykut, G. A. & McPhee, M. G. Solar heating of the Arctic mixed layer. *J. Geophys. Res. Oceans* **100**, 24691–24703 (1995).

8. Hu, S., Zhang, L. & Qian, S. Marine heatwaves in the Arctic region: variation in different ice covers. *Geophys. Res. Lett.* **47**, e2020GL089329 (2020).

9. Huang, B. et al. Prolonged marine heatwaves in the Arctic: 1982–2020. *Geophys. Res. Lett.* **48**, e2021GL095590 (2021).

10. Mohamed, B., Nilsen, F. & Skogseth, R. Marine heatwaves characteristics in the Barents Sea based on high resolution satellite data (1982–2020). *Front. Mar. Sci.* **9**, 821646 (2022).

11. Carvalho, K., Smith, T. & Wang, S. Bering Sea marine heatwaves: patterns, trends and connections with the Arctic. *J. Hydrol.* **600**, 126462 (2021).

12. Kraineva, M. & Golubeva, E. in *Processes in GeoMedia* Vol. V (ed. Chaplina, T.) 169–178 (Springer, 2022).

13. Golubeva, E., Kraineva, M., Platov, G., Iakshina, D. & Tarkhanova, M. Marine heatwaves in Siberian Arctic seas and adjacent region. *Remote Sens.* **13**, 4436 (2021).

14. Suryan, R. M. et al. Ecosystem response persists after a prolonged marine heatwave. *Sci. Rep.* **11**, 6235 (2021).

15. Napp, J. M. & Hunt, G. L. Jr. Anomalous conditions in the south-eastern Bering Sea 1997: linkages among climate, weather, ocean, and biology. *Fish. Oceanogr.* **10**, 61–68 (2001).

16. Mills, K. E. et al. Fisheries management in a changing climate: lessons from the 2012 ocean heat wave in the Northwest Atlantic. *Oceanography* **26**, 191–195 (2013).

17. Szuwalski, C. S., Aydin, K., Fedewa, E. J., Garber-Yonts, B. & Litzow, M. A. The collapse of eastern Bering Sea snow crab. *Science* **382**, 306–310 (2023).

18. Montie, S., Thomsen, M. S., Rack, W. & Broady, P. A. Extreme summer marine heatwaves increase chlorophyll *a* in the Southern Ocean. *Antarct. Sci.* **32**, 508–509 (2020).

19. Latorre, M. P. et al. Summer heatwaves affect coastal Antarctic plankton metabolism and community structure. *J. Exp. Mar. Biol. Ecol.* **567**, 151926 (2023).

20. Hayashida, H., Matear, R. J. & Strutton, P. G. Background nutrient concentration determines phytoplankton bloom response to marine heatwaves. *Glob. Change Biol.* **26**, 4800–4811 (2020).

21. Arteaga, L. A. & Rousseaux, C. S. Impact of Pacific Ocean heatwaves on phytoplankton community composition. *Commun. Biol.* **6**, 263 (2023).

22. Smale, D. A. et al. Marine heatwaves threaten global biodiversity and the provision of ecosystem services. *Nat. Clim. Change* **9**, 306–312 (2019).

23. Gruber, N., Boyd, P. W., Frölicher, T. L. & Vogt, M. Biogeochemical extremes and compound events in the ocean. *Nature* **600**, 395–407 (2021).

24. Holbrook, N. J. et al. A global assessment of marine heatwaves and their drivers. *Nat. Commun.* **10**, 2624 (2019).

25. Hayashida, H., Matear, R. J., Strutton, P. G. & Zhang, X. Insights into projected changes in marine heatwaves from a high-resolution ocean circulation model. *Nat. Commun.* **11**, 4352 (2020).

26. Pilo, G. S., Holbrook, N. J., Kiss, A. E. & Hogg, A. M. Sensitivity of marine heatwave metrics to ocean model resolution. *Geophys. Res. Lett.* **46**, 14604–14612 (2019).

27. Chang, P. et al. An unprecedented set of high-resolution earth system simulations for understanding multiscale interactions in climate variability and change. *J. Adv. Model. Earth Syst.* **12**, e2020MS002298 (2020).

28. Eyring, V. et al. Overview of the Coupled Model Intercomparison Project Phase 6 (CMIP6) experimental design and organization. *Geosci. Model Dev.* **9**, 1937–1958 (2016).

29. IPCC. *Special Report on the Ocean and Cryosphere in a Changing Climate* (eds Pörtner, H.-O. et al.) (Cambridge Univ. Press, 2019).

30. Oliver, E. C. Mean warming not variability drives marine heatwave trends. *Clim. Dynam.* **53**, 1653–1659 (2019).

31. Amaya, D. J. et al. Marine heatwaves need clear definitions so coastal communities can adapt. *Nature* **616**, 29–32 (2023).

32. Donelson, J. M. et al. Understanding interactions between plasticity, adaptation and range shifts in response to marine environmental change. *Philos. Trans. R. Soc. B* **374**, 20180186 (2019).

33. Leu, E. et al. Arctic spring awakening–steering principles behind the phenology of vernal ice algal blooms. *Prog. Oceanogr.* **139**, 151–170 (2015).

34. KAHRU, M., Brotas, V., Manzano-Sarabia, M. & Mitchell, B. Are phytoplankton blooms occurring earlier in the Arctic? *Glob. Change Biol.* **17**, 1733–1739 (2011).

35. Brown, J. H., Gillooly, J. F., Allen, A. P., Savage, V. M. & West, G. B. Toward a metabolic theory of ecology. *Ecology* **85**, 1771–1789 (2004).

36. Pörtner, H. O. et al. Trade-offs in thermal adaptation: the need for a molecular to ecological integration. *Physiol. Biochem. Zool.* **79**, 295–313 (2006).

37. Wolf, K. K. E. et al. Heatwave responses of Arctic phytoplankton communities are driven by combined impacts of warming and cooling. *Sci. Adv.* **10**, eadl5904 (2024).

38. Gutow, L., Petersen, I., Bartl, K. & Huenerlage, K. Marine meso-herbivore consumption scales faster with temperature than seaweed primary production. *J. Exp. Mar. Biol. Ecol.* **477**, 80–85 (2016).

39. Chen, B., Landry, M. R., Huang, B. & Liu, H. Does warming enhance the effect of microzooplankton grazing on marine phytoplankton in the ocean? *Limnol. Oceanogr.* **57**, 519–526 (2012).

40. Liu, K. et al. What controls microzooplankton biomass and herbivory rate across marginal seas of China? *Limnol. Oceanogr.* **66**, 61–75 (2021).

41. Niedzwiedz, S., Diehl, N., Fischer, P. & Bischof, K. Seasonal and inter-annual variability in the heatwave tolerance of the kelp *Saccharina latissima* (Laminariales, Phaeophyceae). *Phycol. Res.* **70**, 212–222 (2022).

42. Samuels, T., Rynearson, T. A. & Collins, S. Surviving heatwaves: thermal experience predicts life and death in a Southern Ocean diatom. *Front. Mar. Sci.* **8**, 600343 (2021).

43. Bozzato, D., Jakob, T. & Wilhelm, C. Effects of temperature and salinity on respiratory losses and the ratio of photosynthesis to respiration in representative Antarctic phytoplankton species. *PLoS ONE* **14**, e0224101 (2019).

44. López-Urrutia, Á., San Martin, E., Harris, R. P. & Irigoien, X. Scaling the metabolic balance of the oceans. *Proc. Natl Acad. Sci. USA* **103**, 8739–8744 (2006).

45. Alcaraz, M., Felipe, J., Grote, U., Arashkevich, E. & Nikishina, A. Life in a warming ocean: thermal thresholds and metabolic balance of arctic zooplankton. *J. Plankton Res.* **36**, 3–10 (2013).

46. Barbeaux, S. J., Holsman, K. & Zador, S. Marine heatwave stress test of ecosystem-based fisheries management in the Gulf of Alaska Pacific cod fishery. *Front. Mar. Sci.* **7**, 703 (2020).

47. Leles, S. G. & Levine, N. M. Mechanistic constraints on the trade-off between photosynthesis and respiration in response to warming. *Sci. Adv.* **9**, eadh8043 (2023).

48. Abele, D. & Puntarulo, S. Formation of reactive species and induction of antioxidant defence systems in polar and temperate marine invertebrates and fish. *Comp. Biochem. Physiol. A* **138**, 405–415 (2004).

49. Grote, U., Pasternak, A., Arashkevich, E., Halvorsen, E. & Nikishina, A. Thermal response of ingestion and egestion rates in the Arctic copepod *Calanus glacialis* and possible metabolic consequences in a warming ocean. *Polar Biol.* **38**, 1025–1033 (2015).

50. Søreide, J. E., Leu, E., Berge, J., Graeve, M. & Falk-Petersen, S. Timing of blooms, algal food quality and *Calanus glacialis* reproduction and growth in a changing Arctic. *Glob. Change Biol.* **16**, 3154–3163 (2010).

51. Laurel, B. J. et al. Regional warming exacerbates match/mismatch vulnerability for cod larvae in Alaska. *Prog. Oceanogr.* **193**, 102555 (2021).

52. Polyakov, I. V. et al. Borealization of the Arctic Ocean in response to anomalous advection from sub-Arctic seas. *Front. Mar. Sci.* **7**, 491 (2020).

53. McCabe, R. M. et al. An unprecedented coastwide toxic algal bloom linked to anomalous ocean conditions. *Geophys. Res. Lett.* **43**, 10,366–310,376 (2016).

54. Guibourd de Luzinais, V., Gascuel, D., Reygondeau, G. & Cheung, W. W. L. Large potential impacts of marine heatwaves on ecosystem functioning. *Glob. Change Biol.* **30**, e17437 (2024).

55. Deguette, A., Barrote, I. & Silva, J. Physiological and morphological effects of a marine heatwave on the seagrass *Cymodocea nodosa*. *Sci. Rep.* **12**, 7950 (2022).

56. Siegel, D. A., DeVries, T., Cetinić, I. & Bisson, K. M. Quantifying the ocean's biological pump and its carbon cycle impacts on global scales. *Annu. Rev. Mar. Sci.* **15**, 329–356 (2023).

57. Rehder, L., Rost, B. & Rokitta, S. D. Abrupt and acclimation responses to changing temperature elicit divergent physiological effects in the diatom *Phaeodactylum tricornutum*. *New Phytol.* **239**, 1005–1013 (2023).

58. Landry, M. R., Freibott, A. L., Beatty, J. L. & Selph, K. E. Phytoplankton biomass responses to a marine heat wave align with altered nitracline depth. *Limnol. Oceanogr.* **69**, 1683–1694 (2024).

59. Richaud, B. et al. Drivers of marine heatwaves in the Arctic Ocean. *J. Geophys. Res. Oceans* **129**, e2023JC020324 (2024).

60. Stewart, K. D. & Haine, T. W. Thermobaricity in the transition zones between alpha and beta oceans. *J. Phys. Oceanogr.* **46**, 1805–1821 (2016).

61. Sen Gupta, A. et al. Drivers and impacts of the most extreme marine heatwave events. *Sci. Rep.* **10**, 19359 (2020).

62. Wassmann, P. & Reigstad, M. Future Arctic Ocean seasonal ice zones and implications for pelagic–benthic coupling. *Oceanography* **24**, 220–231 (2011).

63. Worden, A. Z. et al. Rethinking the marine carbon cycle: factoring in the multifarious lifestyles of microbes. *Science* **347**, 1257594 (2015).

64. Zhang, F., He, J., Lin, L. & Jin, H. Dominance of picophytoplankton in the newly open surface water of the central Arctic Ocean. *Polar Biol.* **38**, 1081–1089 (2015).

65. Tremblay, G. et al. Late summer phytoplankton distribution along a 3500 km transect in Canadian Arctic waters: strong numerical dominance by picoeukaryotes. *Aquat. Microb. Ecol.* **54**, 55–70 (2009).

66. Iriarte, J. L. & Gonzalez, H. E. Phytoplankton size structure during and after the 1997/98 El Niño in a coastal upwelling area of the northern Humboldt current system. *Mar. Ecol. Prog. Ser.* **269**, 83–90 (2004).

67. Kudela, R. M., Cochlan, W. P., Peterson, T. D. & Trick, C. G. Impacts on phytoplankton biomass and productivity in the Pacific Northwest during the warm ocean conditions of 2005. *Geophys. Res. Lett.* https://doi.org/10.1029/2006GL026772 (2006).

68. Walsh, J. E. et al. The high latitude marine heat wave of 2016 and its impacts on Alaska. *Bull. Am. Meteorol. Soc.* **99**, S39–S43 (2018).

69. Jones, T. et al. Massive mortality of a planktivorous seabird in response to a marine heatwave. *Geophys. Res. Lett.* **45**, 3193–3202 (2018).

70. Husson, B. et al. Successive extreme climatic events lead to immediate, large-scale, and diverse responses from fish in the Arctic. *Glob. Change Biol.* **28**, 3728–3744 (2022).

71. Tremblay, J.-É. et al. Global and regional drivers of nutrient supply, primary production and CO$_2$ drawdown in the changing Arctic Ocean. *Prog. Oceanogr.* **139**, 171–196 (2015).

72. Ardyna, M. & Arrigo, K. R. Phytoplankton dynamics in a changing Arctic Ocean. *Nat. Clim. Change* **10**, 892–903 (2020).

73. Qi, D. et al. Climate change drives rapid decadal acidification in the Arctic Ocean from 1994 to 2020. *Science* **377**, 1544–1550 (2022).

74. Yamamoto-Kawai, M., McLaughlin, F. A., Carmack, E. C., Nishino, S. & Shimada, K. Aragonite undersaturation in the Arctic Ocean: effects of ocean acidification and sea ice melt. *Science* **326**, 1098–1100 (2009).

75. Hoppe, C. J. M., Wolf, K. K. E., Schuback, N., Tortell, P. D. & Rost, B. Compensation of ocean acidification effects in Arctic phytoplankton assemblages. *Nat. Clim. Change* **8**, 529–533 (2018).

76. Burger, F. A., Terhaar, J. & Frölicher, T. L. Compound marine heatwaves and ocean acidity extremes. *Nat. Commun.* **13**, 4722 (2022).

77. Gosselin, M., Levasseur, M., Wheeler, P. A., Horner, R. A. & Booth, B. C. New measurements of phytoplankton and ice algal production in the Arctic Ocean. *Deep Sea Res. II* **44**, 1623–1644 (1997).

78. Fernández-Méndez, M. et al. Photosynthetic production in the central Arctic Ocean during the record sea-ice minimum in 2012. *Biogeosciences* **12**, 3525–3549 (2015).

79. Kohlbach, D. et al. The importance of ice algae-produced carbon in the central Arctic Ocean ecosystem: food web relationships revealed by lipid and stable isotope analyses. *Limnol. Oceanogr.* **61**, 2027–2044 (2016).

Methods

Climate model

The high-resolution model used in this study is based on CESM 1.3 (ref. [80]). It has a nominal horizontal resolution of 0.1° in the ocean and sea ice components and 0.25° in the atmosphere and land components. Vertically the model uses a z coordinate with 62 layers and the top 200 m is divided by 20 layers with an interval of 10 m. The oceanic eddies are unparameterized in this model. The riverine input to the ocean is simulated using a river transport model that is synchronously coupled to the land component of the CESM model (CLM4; ref. [81]) for hydrological applications as well as for improved land–ocean–sea ice–atmosphere coupling in the CESM. The time period for study is 1950–2100, with 1950–2005 and 2006–2100, respectively, applied with historical forcing and RCP 8.5 forcing (high CO_2 emission scenario)[82]. The spin-up time is 250 years, with climate forcings fixed to 1850 conditions. We use the daily outputs to analyse the properties of, and impacts from, MHWs. The detailed set up of the model can be found in an overview paper[27], and the way to run the high-resolution model is documented in ref. [80].

The model outperforms the CMIP5 ensemble (with low resolution) and a low-resolution analogue model in the simulation of non-polar MHWs[83]. The intensity and frequency of the model MHWs are closer to the observations. The future projection of non-polar MHWs in our model is quite different from the low-resolution models, and therefore high-resolution models are necessary for projecting future MHWs, also in the Arctic. Furthermore, the high-resolution model simulates more accurate paths of ocean currents compared to the low-resolution model due to the resolving of boundary currents and ocean eddies. As a result of such influences from ocean heat transport, the spatial patterns of the sea ice edge are more realistic in high-resolution models (ref. [27]; Supplementary Fig. 1c–f). Therefore, future Arctic MHWs emerging with retreating sea ice have more reliable locations in high-resolution models. It is worth noting that the amount of Arctic sea ice is generally less in high-resolution models[27,84], and there is no consensus about whether high- or low-resolution models are more consistent with observations[84]. In this case, the SIC in our high-resolution model is at the lower limit of observational results, but capable of simulating the seasonal and interannual variability (Supplementary Fig. 1a,b). Another note is that the high-resolution model simulates a 2 °C higher SST on the Arctic shelves compared to a low-resolution analogue version[27], probably related to a higher ocean heat transport to Arctic[27], as also a general case for the high-resolution models[85].

Observation-based dataset

The daily SST data from the operational sea surface temperature and ice analysis (OSTIA)[86], provided by the UK Met Office, is used for calculating the observational MHW. This dataset has an advantage of high horizontal resolution (1/20°).The time span is from 1988 to 2022. This dataset is a combination of observations from satellite data and in situ observations.

Marine heatwaves

The definition of MHW and its properties basically follows ref. [87]. The MHW is defined as an extreme warming event lasting for at least 5 days of which SST exceeds a 90% threshold. This definition is specific for surface MHWs, please note that MHWs can also occur in the subsurface[88]. Gaps no longer than 2 days with the subsequent at least 5 days exceeding the threshold are recognized as a continuous MHW. The threshold for the model is calculated by the data of an 11 day window within a 31 year moving baseline, with the day and year for calculation centred on the window and baseline, respectively. It is then applied by a 31 day running mean for smoothing. The threshold for the observational dataset is the same, except for the baseline covering the whole period (1982–2022), given that the time span is too short to make moving baselines. The moving baseline is suitable for the future warming scenario as excluding the MHWs induced by the background warming

instead of the change in extreme variability[1]. On the basis of the definition, the calculation for the model is based on the daily SST from 1950 to 2100 but the results exclude the first and last 15 years of 1950–2100. The analyses presented in this study are thus for the time period 1965–2085. We apply the same baseline to the model period of 1982–2022 as the observational dataset would result in more substantial increasing trends of MHW properties in the model, being more comparable to the observational MHW properties (Fig. 1c and Extended Data Figs. 2–4c).

The MHWs are identified on the basis of consecutive daily time series over the entire years, and thus the start and end dates of MHWs can be in different months. For the MHW properties, since this study focuses on the summer season (JJA), the cumulative intensity is the integral of the SST anomaly over all MHW days in JJA and the cumulative duration is the number of MHW days within JJA. The cumulative intensity in other seasons presented in Extended Data Fig. 1 follows the same calculation. The maximum intensity denotes the maximum SST anomaly above threshold during an MHW. The abruptness during development phase is defined as the difference of SST anomaly above the threshold between the start of MHW and day of maximum intensity divided by the number of days. The reason for not using the absolute SST in defining the abruptness is that the absolute SST includes the climatological seasonal cycle. The annual means of maximum intensity, abruptness and duration per event are averaged for the number of MHWs with end dates in JJA, which is counted as the frequency. The area averaging for the time series is based on summer-mean SIC north of 60° N. The mean state of cumulative intensity, cumulative duration and frequency is the average of annual JJA means, and that of the other properties is the average of all the MHW events with end dates in JJA.

The time series of cumulative duration and frequency show strong stochasticity and vary in the range of 0–30 days and 0–1 occurrences per summer season (JJA), respectively (Supplementary Fig. 2c,f). The magnitude of both properties is larger when sea ice cover is lower. The duration per MHW (Extended Data Fig. 5c) is relatively constant over time (10–20 days) for regions of SIC < 50%. For regions of SIC > 50%, it shows a slightly lower magnitude (10–15 days). The large fluctuations and missing values in the latter half of the period are related to less to no occurrences of MHWs due to generally lower sea ice cover, which are shown by near-zero values in the time series of cumulative duration and frequency. This also applies to the large fluctuations and missing values in the time series of maximum intensity (Extended Data Fig. 6c). The spatial patterns of mean state and trend of maximum intensity (Extended Data Fig. 6a,b) are similar to those of cumulative intensity (Fig. 2c,d). The maximum intensity also increases with a decrease in sea ice. It is close to 0 °C where SIC > 85% and varies in the ranges of 0.2–0.7 °C and 0.7–1.2 °C when SIC is 50–85% and <50%, respectively (Extended Data Fig. 6c).

Stratification

The stratification in the upper 50 m (Fig. 4a) is represented by the buoyancy frequency N^2 calculated with density difference between 50 m and the surface. The reason for using the difference between just two layers and masking where the depth is shallower than 50 m (Figs. 4 and 5) is because daily outputs in the upper 50 m are only saved at these two layers. A caveat is that the summer MLD in the Arctic Ocean could be different from 50 m (for example, <50 m in the Canada Basin[89]), and thus the stratification change properly suggests the change in nutrient replenishment at where the MLD is around 50 m.

$$N^2 = -\frac{g}{\rho_0}\frac{\partial \rho}{\partial z}$$

The temperature and salinity effects on the stratification are represented, respectively, by N_θ^2 and N_S^2 (refs. [90,91])

$$N_\theta^2 = g\alpha\frac{\partial \theta}{\partial z}$$

$$N_S^2 = -g\beta \frac{\partial S}{\partial z}$$

where $g = 9.8$ m s^{-2} is gravitational acceleration, $\rho_0 = 1{,}025$ kg m^{-3} is seawater density; α and β are, respectively, thermal expansion coefficient and haline contraction coefficient; and ρ, θ and S are, respectively, potential density, potential temperature and salinity.

The SCI is defined as[90]

$$SCI = \frac{N_\theta^2 - N_S^2}{N_\theta^2 + N_S^2}$$

When SCI ≥ 1, the ocean is stratified by temperature and destratified by salinity. When SCI ≤ -1, the ocean is stratified by salinity and destratified by temperature. When $-1 \leq$ SCI ≤ 1, the ocean is stratified by both temperature and salinity. The transitions occur when SCI $= 1$ (no salinity stratification) and SCI $= -1$ (no temperature stratification).

Regarding the decrease in stratification and increase in MLD during MHWs in some regions (Fig. 4a,b), it may be connected to a generally shallower MLD in these regions (5 m) (Supplementary Fig. 3c,d) and the MLD has generally increased from 1970–1999 to 2010–2019 in a hindcast model, probably as a result of higher wind-induced momentum input with sea ice loss[92]. As MHWs intensify with sea ice retreat, the greater open-ocean area leads to enhanced wind-induced mixing, thereby reducing the MHW-related increase in stratification (due to meltwater input and temperature increase). This is also the reason for the negative anomaly of salinity effects on stratification during MHWs (Fig. 5g,h). Nevertheless, after the complete disappearance of sea ice, an increase in stratification with MHW can be expected also for those regions. In the central Arctic, however, the MLD under the influence of warming-induced sea ice melt is deeper (-15 m; Supplementary Fig. 3e). This region is therefore less susceptible to wind-stress-driven deepening of the MLD in the absence of sea ice, and the MHWs are accompanied with stronger stratification and a shallower MLD by about half the interannual variability (Fig. 4c,d).

Statistics

Linear trends are calculated by linear least-squares regression based on annual-mean data, multiplied by 10 for the linear decadal trends. The composite-mean difference from daily climatology to MHW day and that standardized by interannual standard deviation are, respectively, defined as[20]

$$\text{Diff}(\text{lon}, lat) = \frac{1}{D(\text{lon}, lat)} \sum_D (c - c_{DC})$$

$$\text{Diff}_{stand}(\text{lon}, lat) = \frac{1}{D(\text{lon}, lat)} \sum_D \frac{(c - c_{DC})}{c_{SD}}$$

where lon and lat denote longitudes and latitudes, respectively, c is stratification/MLD and a function of longitudes and latitudes, D is total number of days with MHW, the subscripts DC and SD, respectively, denote daily climatology mean and interannual standard deviation based on the days of MHW date during the 31 year moving baseline.

$$\text{Diff}(\text{lon}, lat) = \frac{1}{D(\text{lon}, lat)} \sum_D (c - c_{DC})$$

$$\text{Diff}_{stand}(\text{lon}, lat) = \frac{1}{D(\text{lon}, lat)} \sum_D \frac{(c - c_{DC})}{c_{SD}}$$

Data availability

The model outputs are available from https://ihesp.github.io/archive/products/ds_archive/Sunway_Runs.html. The OSTIA dataset is available at https://ghrsst-pp.metoffice.gov.uk/ostia-website/index.html. The observational datasets of SIC can be retrieved and downloaded from https://climexp.knmi.nl//selectfield_obs2.cgi?id=eeb887be241d13437b916d8e47749509.

Code availability

The model code is available via Zenodo at https://doi.org/10.5281/zenodo.3637771 (ref. 93). All the other codes used in the data process and visualization are available upon request.

References

80. Zhang, S. et al. Optimizing high-resolution Community Earth System Model on a heterogeneous many-core supercomputing platform. *Geosci. Model Dev.* **13**, 4809–4829 (2020).
81. Lawrence, D. M. et al. Parameterization improvements and functional and structural advances in Version 4 of the Community Land Model. *J. Adv. Model. Earth Syst.* https://doi.org/10.1029/2011MS00045 (2011).
82. IPCC. *Climate Change 2021: The Physical Science Basis* (eds Masson-Delmotte, V. et al.) (Cambridge Univ. Press, 2021).
83. Guo, X. et al. Threat by marine heatwaves to adaptive large marine ecosystems in an eddy-resolving model. *Nat. Clim. Change* **12**, 179–186 (2022).
84. Selivanova, J., Iovino, D. & Cocetta, F. Past and future of the Arctic sea ice in high-resolution model intercomparison project (HighResMIP) climate models. *Cryosphere* **18**, 2739–2763 (2024).
85. Docquier, D. et al. Impact of model resolution on Arctic sea ice and North Atlantic Ocean heat transport. *Clim. Dynam.* **53**, 4989–5017 (2019).
86. Good, S. et al. The current configuration of the OSTIA system for operational production of foundation sea surface temperature and ice concentration analyses. *Remote Sens.* **12**, 720 (2020).
87. Hobday, A. J. et al. A hierarchical approach to defining marine heatwaves. *Prog. Oceanogr.* **141**, 227–238 (2016).
88. Sun, D., Li, F., Jing, Z., Hu, S. & Zhang, B. Frequent marine heatwaves hidden below the surface of the global ocean. *Nat. Geosci.* **16**, 1099–1104 (2023).
89. Toole, J. M. et al. Influences of the ocean surface mixed layer and thermohaline stratification on Arctic Sea ice in the central Canada Basin. *J. Geophys. Res. Oceans* https://doi.org/10.1029/2009JC005660 (2010).
90. Caneill, R., Roquet, F., Madec, G. & Nycander, J. The polar transition from alpha to beta regions set by a surface buoyancy flux inversion. *J. Phys. Oceanogr.* **52**, 1887–1902 (2022).
91. Carmack, E. C. The alpha/beta ocean distinction: a perspective on freshwater fluxes, convection, nutrients and productivity in high-latitude seas. *Deep Sea Res. II* **54**, 2578–2598 (2007).
92. Hordoir, R. et al. Changes in Arctic stratification and mixed layer depth cycle: a modeling analysis. *J. Geophys. Res. Oceans* **127**, e2021JC017270 (2022).
93. RUO. lgan/cesm_sw_1.0.1: some efforts on refactoring and optimizing the Community Earth System Model(CESM1.3.1) on the Sunway TaihuLight supercomputer (cesm_sw_1.0.1). *Zenodo* https://doi.org/10.5281/zenodo.3637771 (2020).

Competing interests

The authors declare no competing interests.

Additional information

Extended data is available for this paper at https://doi.org/10.1038/s41558-024-02224-7.

Supplementary information The online version contains supplementary material available at https://doi.org/10.1038/s41558-024-02224-7.

Correspondence and requests for materials should be addressed to Ruijian Gou.

Peer review information *Nature Climate Change* thanks Benjamin Richaud and the other, anonymous, reviewer(s) for their contribution to the peer review of this work.

**Reprints and permissions information** is available at www.nature.com/reprints.
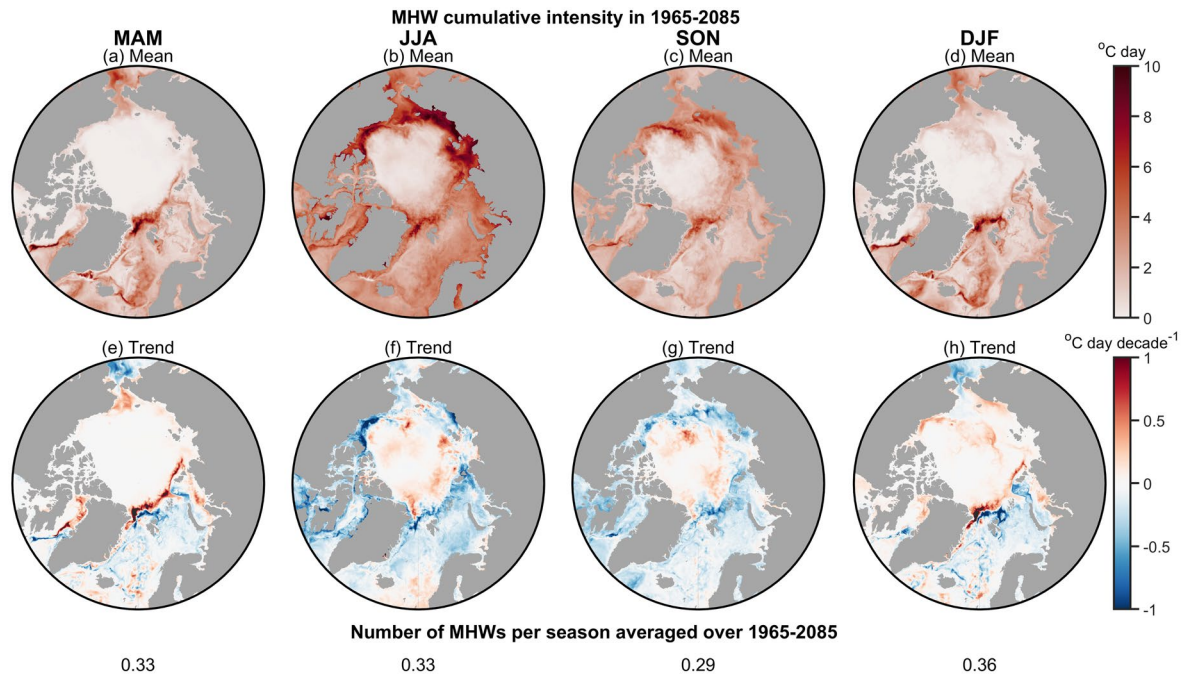
Extended Data Fig. 1 | The seasonality of MHWs. a-d, the mean state of the cumulative intensity averaged over the spring (**a**, MAM – March, April, May), summer (**b**, JJA – June, July, August), autumn (**c**, SON – September, October, November), winter (**d**, DJF – December, January, February) of 1965-2085. **e-h**, the same as (**a-d**) but for the linear decadal trend. The numbers of MHWs per season averaged over the whole period are indicated in the last row.
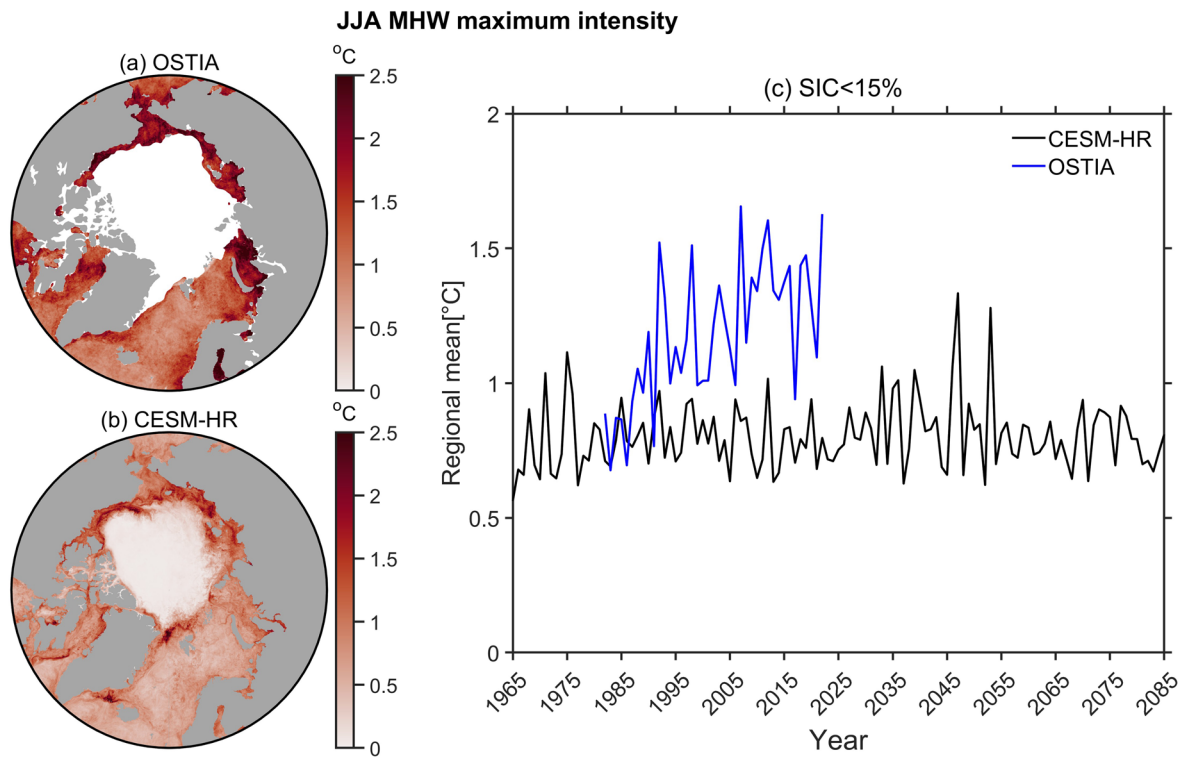
JJA MHW cumulative duration in 1982-2022
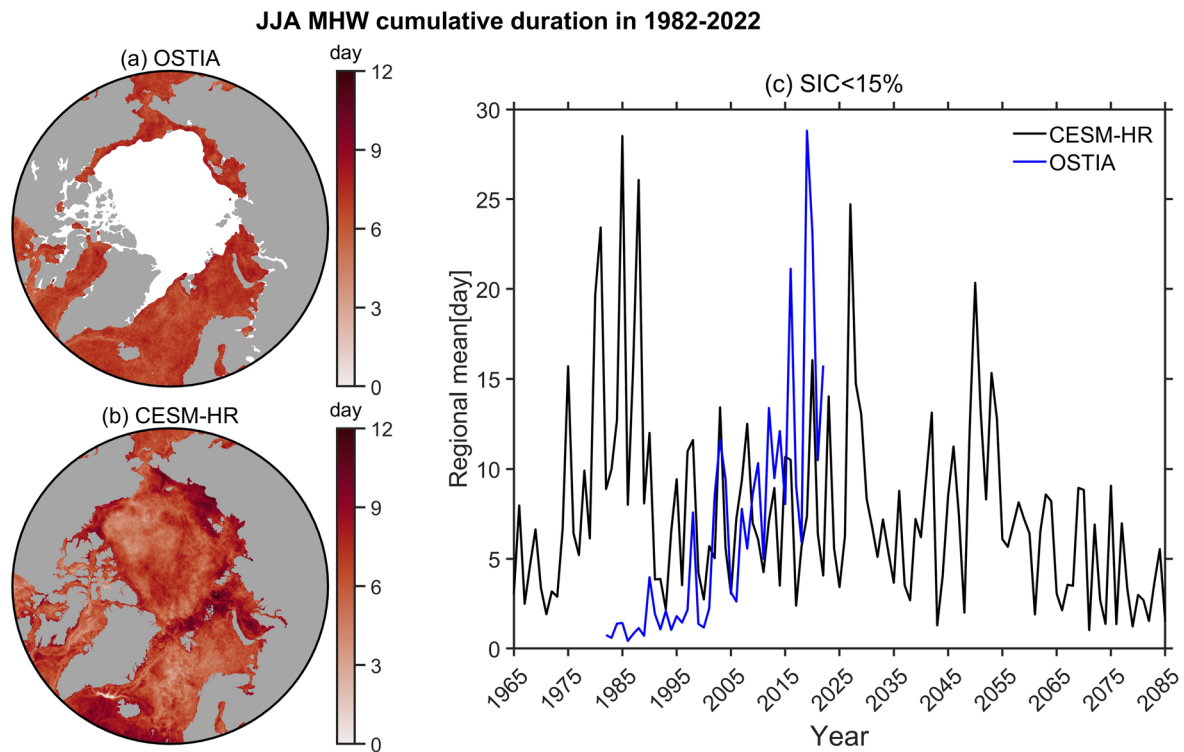
Extended Data Fig. 2 | The cumulative duration of Arctic MHWs in the observational record. a-b, the average over JJA in 1982-2022 for observational dataset (**a**) and the model (**b**). The observational area with SIC above 15% at the end of summer season (average on 31st, August) is masked by white shading. **c**, timeseries of the JJA-mean cumulative duration, averaged over regions with SIC below 15%. The standard deviations of timeseries from the model and observational dataset are respectively 5.29 and 6.66 day.
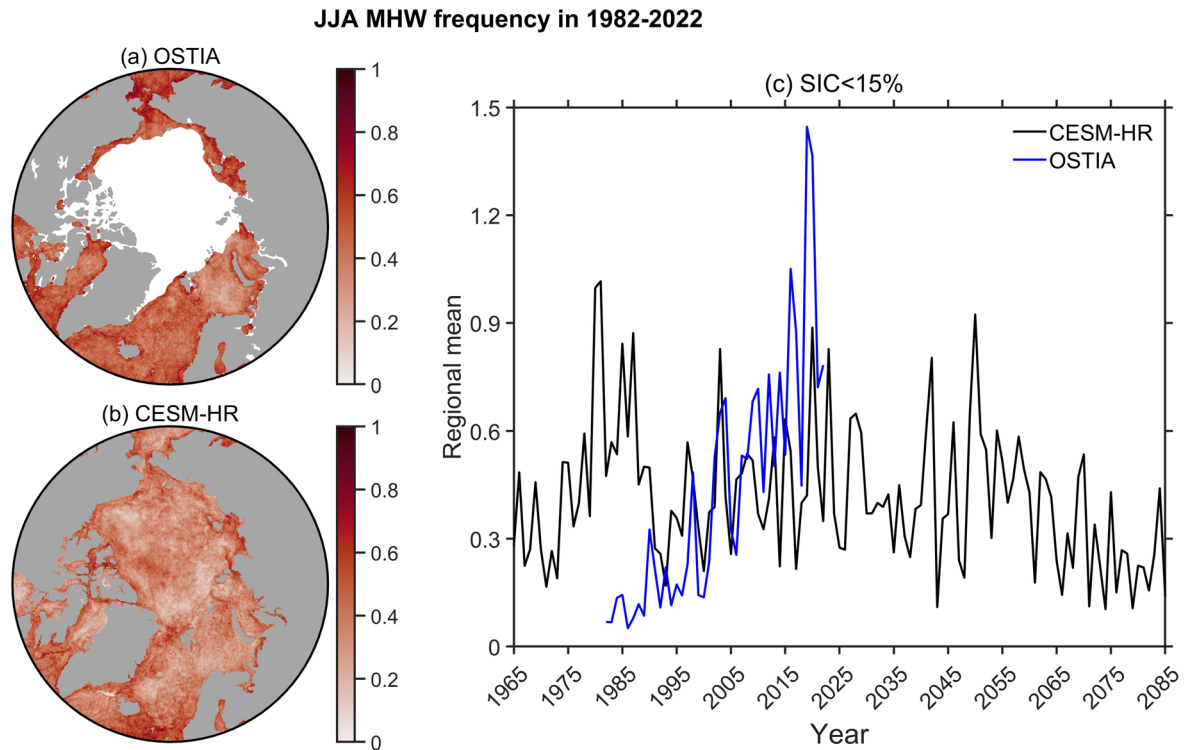
Extended Data Fig. 3 | The frequency of Arctic MHWs in the observational record. a-b, the average over JJA in 1982-2022 for observational dataset (**a**) and the model (**b**). The observational area with SIC above 15% at the end of summer season (average on 31st, August) is masked by white shading. **c**, timeseries of the JJA-mean frequency, averaged over regions with SIC below 15%. The standard deviations of timeseries from the model and observational dataset are respectively 0.19 and 0.35.
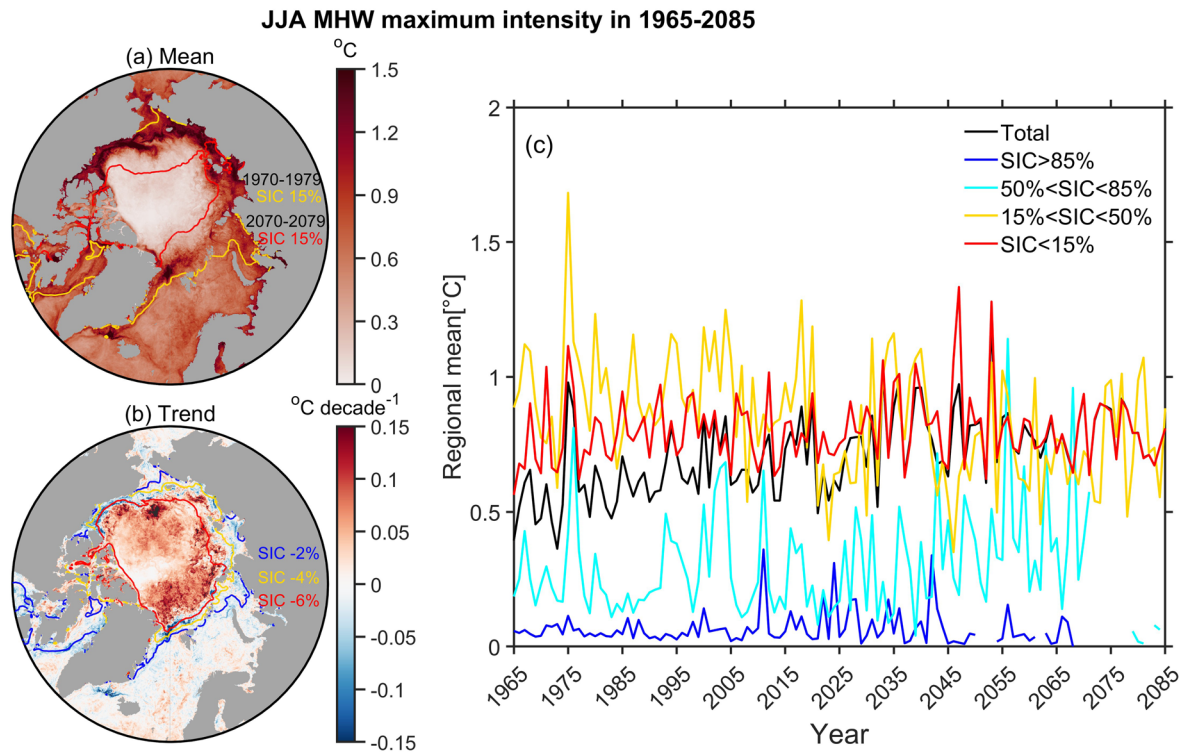
Extended Data Fig. 4 | The maximum intensity of Arctic MHWs in the observational record. a-b, the average of MHWs in JJA 1982-2022 for observational dataset (**a**) and the model (**b**). The observational area with SIC above 15% at the end of summer season (average on 31st, August) is masked by white shading. **c**, timeseries of the JJA-mean maximum intensity, averaged over regions with SIC below 15%. The standard deviations of timeseries from the model and observational dataset are respectively 0.13 and 0.26 °C.

JJA MHW duration per event in 1965-2085

(a) Mean

(b) Trend

(c)
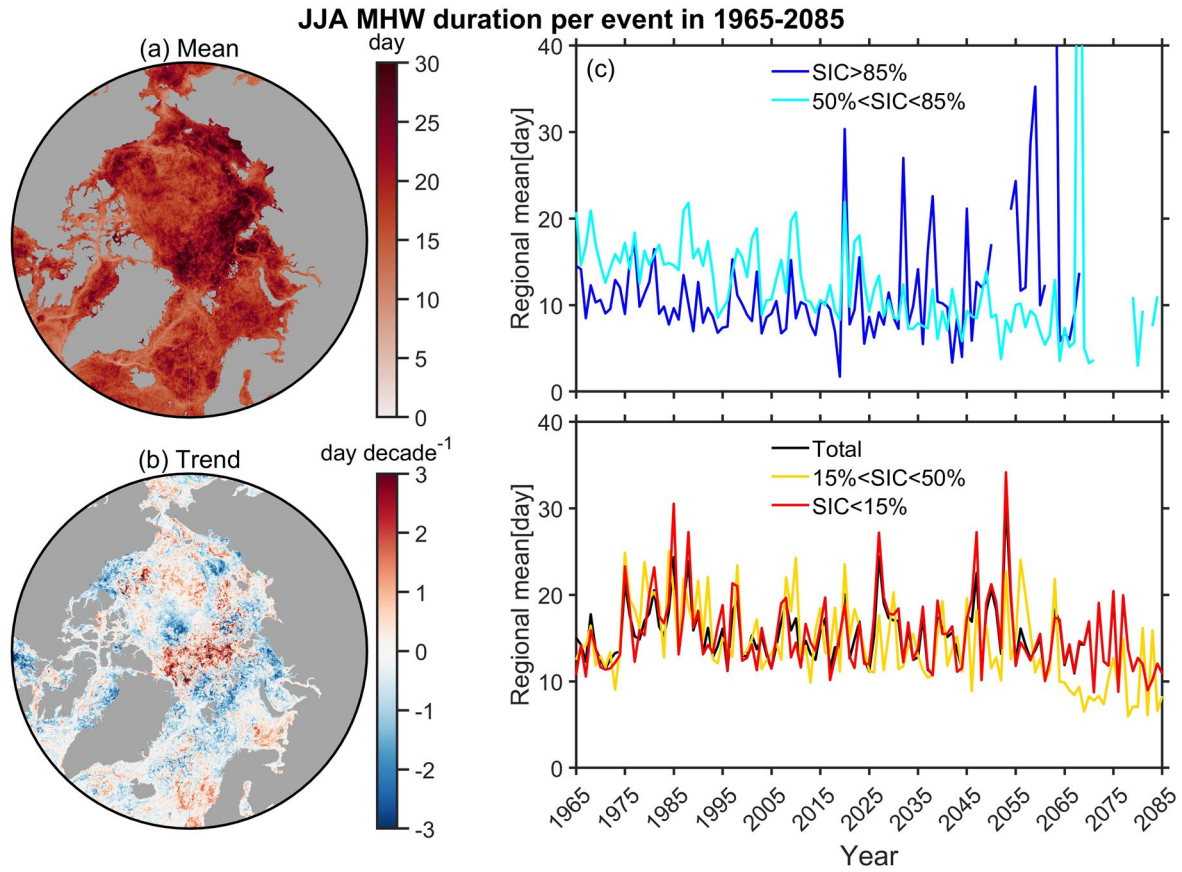
Extended Data Fig. 5 | The duration per Arctic MHW under global warming. a–c, mean state (a), linear decadal trend (b), timeseries (c) of the duration per event over JJA in 1965-2085. The timeseries (annual means) are averaged over regions with certain sea ice concentration, denoted by lines of different color in (c). If a region is free of MHWs in a year, the annual mean is not shown in (c).

JJA MHW maximum intensity in 1965-2085

Extended Data Fig. 6 | The maximum intensity of Arctic MHWs under global warming. a-c, mean state (**a**), linear decadal trend (**b**), timeseries (**c**) of the maximum intensity over JJA in 1965-2085. The timeseries (annual means) are averaged over regions with certain sea ice concentration, denoted by lines of different color in (**c**). If a region is free of MHWs in a year, the annual mean is not shown in (**c**). The yellow and red line in (**a**) denote sea ice concentration of 15% averaged over 1970-1979 and 2070-2079 respectively. The blue, yellow, red lines in (**b**) indicate the linearly decreasing decadal trend of 2%, 4%, 6% respectively.